Synthesis, Structure, and Magnetic Properties of $[Li(H_2O)M(N_2H_3CO_2)_3]\cdot 0.5H_2O$ (M = Co,Ni) as Single Precursors to $LiMO_2$ Battery Materials

Szu Lui Tey,[†] M. V. Reddy,[‡] G. V. Subba Rao,[‡] B. V. R. Chowdari,[‡] Jiabao Yi,[§] Jun Ding,[§] and Jagadese J. Vittal*[,†]

Department of Chemistry, Department of Physics, and Department of Materials Science & Engineering, National University of Singapore, Singapore 117543

Received October 31, 2005. Revised Manuscript Received January 28, 2006

$[Li(H_2O)M(N_2H_3CO_2)_3]\cdot 0.5H_2O$, M = Ni (**1**) and Co (**2**), has been synthesized in moderate yield from the corresponding metal salts and hydrazinecarboxylate anion, $N_2H_3CO_2^-$, prepared by mixing $N_2H_4\cdot H_2O$ and dry ice. Both the compounds crystallized in the chiral space group $P2_1$ and have interesting 2D bilayer network structures in the solid state comprising fused helical coordination polymers with extensive hydrogen bonding. Samples **1** and **2** exhibited paramagnetism, as shown by the variable temperature magnetic measurements. The calculated magnetic moments were 2.82 and 4.39 μ_B for **1** and **2**, respectively. These two compounds have been investigated as single precursors for layered materials $LiMO_2$, M = Ni and Co. Pyrolysis of **1** and **2** yields $LiNiO_2$ and $LiCoO_2$ at 700 °C in an oxygen atmosphere and at $T >$ 700 °C in air, respectively. They were characterized by powder XRD, Rietveld refinement, and SEM. Cathodic properties of $LiMO_2$ have been evaluated by cyclic voltammetry and galvanostatic charge−discharge cycling up to 20 cycles in the voltage ranges, 2.5−4.3 and 2.5−4.5 V vs Li metal. Results are in tune with those reported in the literature, thereby indicating that **1** and **2** are excellent single-source precursors for obtaining electrochemically active battery materials.

Introduction

Since the successful introduction of rechargeable nickel−cadmium and nickel−metal hydride batteries, the search for smaller, lighter, and more powerful sources has inevitably led to the development of lithium-ion battery technology. This is primarily attributed to the growing demand for smaller, more sophisticated, and portable devices. Thus high-energy density power sources are particularly engaged in the fields of communications, computers, electronics, more demanding power tools, and transportation. Lithium-ion batteries (LIB) are appealing for these applications because they are more compact and provide higher energy density compared to other rechargeable battery systems. When nonaqueous electrolytes are used, lithium-ion batteries also offer a wider range of operational temperatures.[1,2] In the lithium-ion cells, the cathode is a transition-metal oxide, typically $LiCoO_2$, $LiMn_2O_4$, or $LiNiO_2$. Different carbon materials, coated on copper foils, serve as the anode. During charging, the lithium cations are removed from the oxide layers and introduced into the space of the graphite layers via an electrolyte containing lithium salts dissolved in organic solvents. The reverse reaction occurs during discharging. Thus, lithium-ion cells show good recycling electrochemical abilities for rechargeable battery materials.[1,2]

The electrochemical properties of double oxides mainly depend on methods of preparation, temperature, and time of heating, and therefore, we have initiated a project to employ a single-precursor route for preparing $LiCoO_2$ and $LiNiO_2$. In the literature, there are several synthetic approaches for preparing $LiNiO_2$ and $LiCoO_2$, namely the solid-state reaction, sol−gel synthesis, ion-exchange, hydrothermal and the newly developed mechanochemistry method,[1−10] polymer precursor,[11] and molten salt synthesis.[12] The solid-state reaction involves heating solid reactant mixtures at high temperatures, but it might not yield high purity products.[1] This phenomenon is attributed to the diffusion limitations of the reactants due to the large particle size and low porosity. Thus, the core of the solid might not undergo a complete reaction. Moreover, it also involves long reaction times and regrinding between subsequent firings.[1] The sol−gel method

* To whom correspondence should be addressed. E-mail: chmjiv@nus.edu.sg. Tel: 65 6516 2975. Fax: 65 6779 1691.
[†] Department of Chemistry, National University of Singapore.
[‡] Department of Physics, National University of Singapore.
[§] Department of Materials Science & Engineering, National University of Singapore.

(1) Nazri, G.-A., Pistoia, G., Eds. *Lithium Batteries: Science and Technology*; Kluwer Academic Publishers: Boston, 2003.
(2) Van Schalkwijk, W. A., Scrosati, B., Eds. *Advances in Lithium-Ion Batteries*; Kluwer Academic/Plenum Publishers: New York, 2002.
(3) Yamada, K.; Sato, N.; Fujino, T.; Lee, C. G.; Uchida, I.; Selman, J. R. *J. Solid State Electrochem.* **1999**, *3*, 148.
(4) Sun, Y.-K.; Oh, I.-H. *J. Mater. Sci. Lett.* **1997**, *16*, 30.
(5) Delmas, C.; Saadoune, I. *Solid State Ionics* **1992**, *53−56*, 370.
(6) Ueda, A.; Ohzuku, T. *Solid State Ionics* **1994**, *69*, 201.
(7) Ohzuku, T.; Ueda, A.; Nagayama, M.; Iwakoshi, Y.; Komori, H. *Electrochim. Acta* **1993**, *38*, 1159.
(8) Rougier, A.; Saadoune, I.; Gravereau, P.; Willmann, P.; Delmas, C. *Solid State Ionics* **1996**, *90*, 83.
(9) Lee, K.-K.; Kim, K.-B. *J. Electrochem. Soc.* **2000**, *147*, 1709.
(10) Arai, H.; Okada, S.; Sakurai, Y.; Yamaki, J.-I. *J. Electrochem. Soc.* **1997**, *144*, 3117.
(11) Li, L.; Meyer, W. H.; Wegner, G.; Wohfahrt-Mehrens, W. *Adv. Mater.* **2005**, *17*, 984.
(12) Tan, K. S.; Reddy, M. V.; Subba Rao, G. V.; Chowdari, B. V. R. *J. Power Sources* **2005**, *147*, 241.

10.1021/cm0523891 CCC: $33.50
Published on Web 02/28/2006

is more superior to the solid-state method because it forms a homogeneous mixture of precursors (gel form) in solution, whereby there is a better control of the stoichiometry, time, and temperature of the reaction.[1,2,4] The desired oxide is obtained upon annealing or solvent-exchange of the precursor. As the sol−gel method enhances control of the reaction parameters, the oxides yield high purity and homogeneity.[1,2,4] Despite the advantages of the above-mentioned methods, both solid-state and sol−gel methods require calcination of reaction mixtures at high temperatures of >800 °C in order to obtain the desired metal double oxide.[1,3,4] Here, we propose the single-source precursor method, which incorporates the advantages of the solution method in the synthesis of the precursor; in this manner, we assured the stoichiometry of the precursor. We have employed hydrazido carbonate anion, $N_2H_3CO_2^-$, as a ligand for synthesizing bimetallic complexes of Ni(II) and Co(II) with Li(I) for this purpose. Several metal complexes of this ligand have been successfully employed for synthesizing the oxide materials.[13−17] Recently, Boyle et al.[18] have used lithium cobalt double aryloxides as single-source precursors to make $LiCoO_2$ thin films. We have now synthesized Ni(II) and Co(II) complexes of a bidentate hydrazido carbonate anion, $N_2H_3CO_2^-$ (which is also known as hydrazine carboxylate anion), namely, $[Li(H_2O)M(N_2H_3CO_2)_3]\cdot 0.5H_2O$, M = Ni (**1**) and Co (**2**). We have characterized their solid-state structures by X-ray crystallography and studied their variable temperature magnetic properties. Further, this paper describes the synthesis and physical and electrochemical characterizations of $LiNiO_2$ and $LiCoO_2$ obtained from these single precursors.

Experimental Section

Synthesis of $[Li(H_2O)Ni(N_2H_3CO_2)_3]\cdot 0.5H_2O$ (1). A solution of $N_2H_3CO_2^-$ was prepared by mixing 1.7 mL (34.4 mmol) of $N_2H_4\cdot H_2O$ and 0.76 g (17.2 mmol) of dry ice and was slowly added to a solution of 1.0 g (3.44 mmol) of $Ni(NO_3)_2\cdot 6H_2O$ and 0.237 g (3.44 mmol) of $LiNO_3$ dissolved in 12 mL of water. The concentration for the Li−Ni salt solution was maintained at approximately 0.28−0.29 mol/L. The reaction mixture was constantly saturated with dry ice and stirred with a magnetic stirrer to obtain a deep blue solution. Slow evaporation of the solution in air yielded purple rodlike crystals that were filtered, washed with acetone and diethyl ether, and vacuum-dried. The deep blue filtrate was then layered with acetonitrile in a 1:1 volume ratio and a second batch of purple crystals was collected. Yield: 0.82 g (77%). Anal. Calcd. for $C_3H_{11}LiN_6NiO_7\cdot 0.5H_2O$ (mol wt 317.84): C, 11.34; H, 3.81; N, 26.44; Li, 2.18. Found: C, 11.34; H, 3.52; N, 26.83; Li, 2.08. Selected IR data: ν(N−N), 1089 (m), 1181(m); ν(C−N) of N−CO2, 1377 (vs), 1464 (vs); ν(C═O), 1606 (s); ν(H−N), 3166 (m) & 3256 (m), 3310 (m); ν(O−H) in hydrogen bonding, 2669 (w) & 2723 (w) cm^{-1}.

Synthesis of $[Li(H_2O)Co(N_2H_3CO_2)_3]\cdot 0.5H_2O$ (2). The synthesis of **2** followed the synthesis method of **1**. However, the metal salt solution was prepared by dissolving 1.0 g (3.44 mmol) of $Co(NO_3)_2\cdot 6H_2O$ and 0.474 g (6.88 mmol) of $LiNO_3$ in 12 mL of water. The reaction mixture gave a deep red solution. The freshly prepared reaction solution was layered with acetonitrile in a 1:1 volume ratio and left to crystallize. Orange-red rodlike single crystals were isolated in the same manner as **1**. Yield: 0.79 g (74%). Anal. Calcd. for $C_3H_{11}LiCoN_6O_7\cdot 0.5H_2O$ (mol wt 318.06): C, 11.33; H, 3.80; N, 26.42; Li, 2.18. Found: C, 11.18; H, 3.62; N, 25.52 and 25.10; Li, 1.86. Selected IR data: ν(N−N), 1084 (m), 1184 (m); ν(C−N) of N−CO2, 1377 (s), 1461 (vs); ν(C═O), 1589 (m); ν(H−N), 3168 (w), 3256(w), 3306 (w); ν(O−H) in hydrogen bonding, 2669 (w), 2724 (w) cm^{-1}.

The precipitation method was carried out for **1** and **2** by adding methanol to the reaction mixture to obtain the products more quickly. However, the precipitates did not contain lithium, as verified by elemental analysis.

Instruments and Characterization. The IR spectra (Nujol mull) were recorded using a Bio-Rad FTIR spectrometer. The elemental analyses were performed by the microanalytical laboratory of the chemistry department, National University of Singapore. Thermogravimetric analyses were carried out using an SDT 2980 TGA thermal analyzer with a heating rate of 10 °C min^{-1} in a N_2 atmosphere using a sample size of 5−10 mg per run. Magnetic susceptibility measurements in the temperature range 5−300 K were carried out with a Quantum Design MPMS-XL5 SQUID. Data were corrected for the magnetism of the sample holder and for the diamagnetic contributions, which were estimated from the Pascal constants.[19] Powder X-ray diffraction (XRD) patterns were obtained using a Siemens D5005 X-ray diffractometer with Cu Kα radiation. Rietveld refinement of XRD data was performed using TOPAS-R (version 2.1). Scanning electron microscope (SEM) images were obtained using a JEOL JSM-5600LV instrument. Cyclic voltammetry at 25 °C was carried out using either the Mac-pile II system (Bio-logic, France) or Solartron battery tester 1470. Galvanostatic cycling tests were carried out using a Bitrode multiple battery tester (Model SCN, Bitrode, USA).

Pyrolysis. Pyrolysis of **1** and **2** was carried out in a quartz or Pyrex glass reactor inside a furnace at a heating rate of 30 °C min^{-1}. Various temperatures and gases employed for **1** at 400 °C were as follows: in air for 1 h; nitrogen flow for 1 h; 0.5 Torr vacuum for 1 h; oxygen for 8 h; and at 700 °C under an oxygen gas flow for 8h. Lithium cobalt precursors were heated at 400, 700, or 850 °C in air, with a heating rate of 3 °C min^{-1}, for 8 h and were finally cooled to room temperature. The obtained products were ground to a fine powder for further analysis.

Electrochemical Studies. Fabrication of the electrodes for electrochemical studies was carried out using a mixture of the following composition: active material (i.e., the respective oxides), super P carbon black (an electronically conducting additive), and polymer binder (Kynar 2801) in the weight ratio 80:10:10. *N*-methyl-pyrrolidone (NMP) was used as the solvent for the binder, and an etched aluminum foil (15 μm thick, Alpha Industries Co. Ltd., Japan) was used as the current collector. Coin-type cells (size 2016) were fabricated in an Ar-filled glovebox (MBraun, Germany) with lithium metal foil as the anode, celgard 2502 as the separator, and 1 M $LiPF_6$ in ethylene carbonate (EC) and diethyl carbonate (DEC) in a 1:1 volume ratio (Merck, Selectipur LP40) as the electrolyte. Details have been described elsewhere.[12,20,21] The

(13) Sekar, M. M. A.; Patil, K. C. *Mater. Res. Bull*. **1993**, *28*, 485.
(14) Ravindranathan, P.; Mahesh, G. V.; Patil, K. C. *J. Solid State Chem.* **1987**, *66*, 20.
(15) Dhas, N. A.; Patil, K. C. *J. Solid State Chem.* **1993**, *102*, 440.
(16) Maèek, J.; Rahten, A. *Thermochim. Acta* **1989**, *144*, 257.
(17) Sivasankar, B. N.; Govindarajan, S. *Synth. React. Inorg. Met.−Org. Chem.* **1995**, *25*, 127.
(18) Boyle, T. J.; Rodriguez, M. A.; Ingersoll, D.; Headley, T. J.; Bunge, S. D.; Pedrotty, D. M.; De'Angeli, S. M.; Vick, S. C.; Fan, H. *Chem. Mater*. **2003**, *15*, 3903.
(19) Khan, O. *Molecular Magnetism*; Wiley-VCH: Weinheim, Germany, 1993.
(20) Reddy, M. V.; Subba Rao, G. V.; Chowdari, B. V. R. *Chem. Mater.* **2006**, submitted.
(21) Tan, K. S.; Reddy, M. V.; Subba Rao, G. V.; Chowdari, B. V. R. *J. Power Sources* **2005**, *141*, 129.

Table 1. Selected Crystal Data and Refinement Details for 1 and 2

	1	2
formula	$C_3H_{12}LiN_6NiO_{7.5}$	$C_3H_{12}CoLiN_6O_{7.5}$
formula mass	317.84	318.06
T (K)	223(2)	223(2)
λ (Å)	0.71073	0.71073
cryst syst	monoclinic	monoclinic
space group	$P2_1$	$P2_1$
a (Å)	9.4868(8)	9.5324(6)
b (Å)	4.9676(4)	5.0019(3)
c (Å)	11.2610(9)	11.3136(7)
β (deg)	92.262(2)	92.337(1)
V (Å^3)	530.28(7)	538.99(6)
Z	2	2
ρ (g cm^3)	1.991	1.960
μ (mm^{-1})	1.877	1.638
θ range (deg)	2.75−29.95	1.80−29.99
total no. of reflns	4176	4354
no. of independent reflns	2775 [R(int) = 0.0200]	2858 [R(int) = 0.0160]
data/restraints/params	2775/47/212	2858/47/212
GOF on F^2	1.063	1.081
final R indices ($I > 2\sigma(I)$)	R1 = 0.0316, wR2 = 0.0787	R1 = 0.0265, wR2 = 0.0735
R indices (all data)	R1 = 0.0330, wR2 = 0.0797	R1 = 0.0270, wR2 = 0.0738
Flack param	0.046(15)	0.026(13)
largest difference peak/hole (e Å^{-3})	0.615 and −0.292	0.644 and −0.292

assembled cells were aged for 24 h at room temperature before being tested.

X-ray Crystallography. The diffraction experiments were carried out on a Bruker SMART CCD diffractometer with Mo Kα radiation from a sealed tube. The SMART[22] program was used for collecting frames of data, indexing reflections, and determining lattice parameters; SAINT[22] was used for integration of the intensity of reflections and scaling. SADABS[23] was used for absorption correction, and SHELXTL[24] was used for space group and structure determination and least-squares refinements on F^2. The relevant crystallographic data and refinement details are shown in Table 1.

Results and Discussion

Synthesis. In the synthesis of **1**, a 1:1 ratio was maintained between Li(I) and Ni(II), whereas a 2-fold excess of Li salts was added to get the desired product of **2**. The salts were dissolved in an excess of $N_2H_5^+$ $N_2H_3CO_2^-$ solution. Further, the reaction mixture was constantly saturated with dry ice and stirred until all the solid was dissolved, giving a clear solution. The crystalline products were isolated by slow evaporation of the solution. On the other hand, the precipitation method yielded light purple nickel and cream-orange cobalt compounds, respectively, for **1** and **2**, but they contain no lithium ion, as found by elemental analysis. It has been found that a 2-fold excess of Li(I) is necessary to incorporate Li in **2** and that the addition of equimolar Co(II) and Li(I) resulted in the formation of $[Co(N_2H_3CO_2)_2(N_2H_4)]$. The observed N−N stretching frequencies, 1089 and 1083 cm^{-1} for **1** and **2**, fall in the range expected for similar reported structures of hydrazine carboxylates.[25−28]

Structural Characterizations of Nickel (1) and Cobalt (2) Complexes. Compounds **1** and **2** have crystallized in chiral space group $P2_1$ and are isomorphous and isostructural. Hence, only the structure of **1** is described in detail. Each metal(II) ion is chelated by three crystallographically independent $N_2H_3CO_2^-$ ligands and thus has a distorted octahedral *fac* NiN_3O_3 core as shown in Figure 1. As a result, the anion exhibits an idealized C_3 symmetry along the *b*-axis. This makes all three C═O groups in the $M(N_2H_3CO_2)_3^-$ anions align in the *ac*-plane to further interact with Li(I). Each Li(I), in turn, is bonded to three C═O oxygen atoms from three neighboring anions and a water molecule. The connectivity between the anions and cations generates helical channels (Figure 1b,c) along the *b*-direction, and the channels are fused together along the *a*-axis to a 2D bilayer network structure as shown in Figure 2. These 2D bilayer brick walls in the *ab*-plane are further joined by extensive hydrogen bonds to form hydrogen-bonded 3D network structures. Such higher-dimensional coordination polymeric structures with chiral channels have been reported in the literature.[29−34] Building chiral materials from achiral building components is a challenging but rewarding problem in materials science.[35] It appears that the presence of *fac* dispositions of the carbonyl oxygen atoms bonded to the Li(I) atoms are responsible for the chiral space group. However, equal amounts of both enantiomers are expected to be present in the crystallization pot. The chemistry of metal complexes of hydrazine and its derivatives is very rich. However, the formation of helical coordination polymeric structures from the achiral $N_2H_3CO_2^-$ anion is unprecedented. Selected metric parameters for **1** and **2** are given in Table 2 that are comparable to those observed for $(N_2H_5)[M(N_2H_3CO_2)_3]\cdot H_2O$ (M = Co, Ni).[36,37]

All the N−H protons are involved in medium-to-weak interactions with the carboxylate oxygen atoms with distances ranging from 2.14 to 2.50 Å except O2. The hydrogen atoms of the aqua ligands are heavily involved in O−H···O with O6 and O8 (oxygen atom of the half lattice water per formula unit in the unit cell; Figure 1a). O2 is strongly hydrogen bonded to the hydrogen atoms of the lattice waters. Table 3 displays selected hydrogen-bond parameters observed in **1** and **2**.

(22) *SMART and SAINT Software Reference Manuals*, version 5.0; Bruker AXS Inc.: Madison, WI, 1998.
(23) Sheldrick, G. M. *SADABS, Software for Empirical Absorption Correction*; University of Göttingen: Göttingen, Germany, 2004.
(24) *SHELXTL Reference Manual*, version 5.1; Bruker AXS Inc.: Madison, WI, 1997.
(25) Braibanti, A.; Dallavalle, F.; Pellinghelli, M. A.; Leporati, E. *Inorg. Chem.* **1968**, *7*, 1430.
(26) Ferrari, A.; Braibanti, A.; Bigliardi, G.; Lanfredi, A. M.; Tiripicchio, A. *Nature* **1996**, *211*, 1174.
(27) Patil, K. C.; Aruna, S. T.; Ekambaram, S. *Curr. Opin. Solid State Mater. Sci.* **1997**, *2*, 158.
(28) Patil, K. C.; Soundararajan, R.; Goldberg, E. P. *Synth. React. Inorg. Met.−Org. Chem.* **1983**, *13*, 29.
(29) Shin, D.; Lee, I. S.; Chung, Y. K. *Inorg. Chem.* **2003**, *42*, 8838.
(30) Luo, J.; Zhou, X. G.; Gao, S.; Weng, L. H.; Shao, Z. H.; Zhang, C. M.; Li, Y. R.; Zhang, J.; Cai, R. F. *Inorg. Chem. Commun.* **2004**, *7*, 669.
(31) Ezuhara, T.; Endo, K.; Aoyama, Y. *J. Am. Chem. Soc.* **1999**, *121*, 3279.
(32) Biradha, K.; Seward, C.; Zaworotko, M. J. *Angew. Chem., Int. Ed.* **1999**, *38*, 492.
(33) Ranford, J. D.; Vittal, J. J.; Wu, D. *Angew. Chem., Int. Ed.* **1998**, *37*, 1114.
(34) Ranford, J. D.; Vittal, J. J.; Wu, D.; Yang, X. *Angew. Chem., Int. Ed.* **1999**, *38*, 3498.
(35) Moulton, B.; Zaworotko, M. J. In *Crystal Engineering: From Molecules and Crystals to Materials*; Braga, D., Grepioni, F., Orpen, A. G., Eds.; Kluwer Academic Publishers: Dordrecht, The Netherlands, 1999; p 311.
(36) Jesih, A.; Rahten, A.; Benkič, P.; Skapin, T.; Pejov, L.; Petruševski, V. M. *J. Solid State Chem.* **2004**, *177*, 4482.
(37) Braibanti, A.; Manotti-Lanfredi, A. M.; Tiripicchio, A. *Z. Kristallogr.* **1967**, *124*, 335.

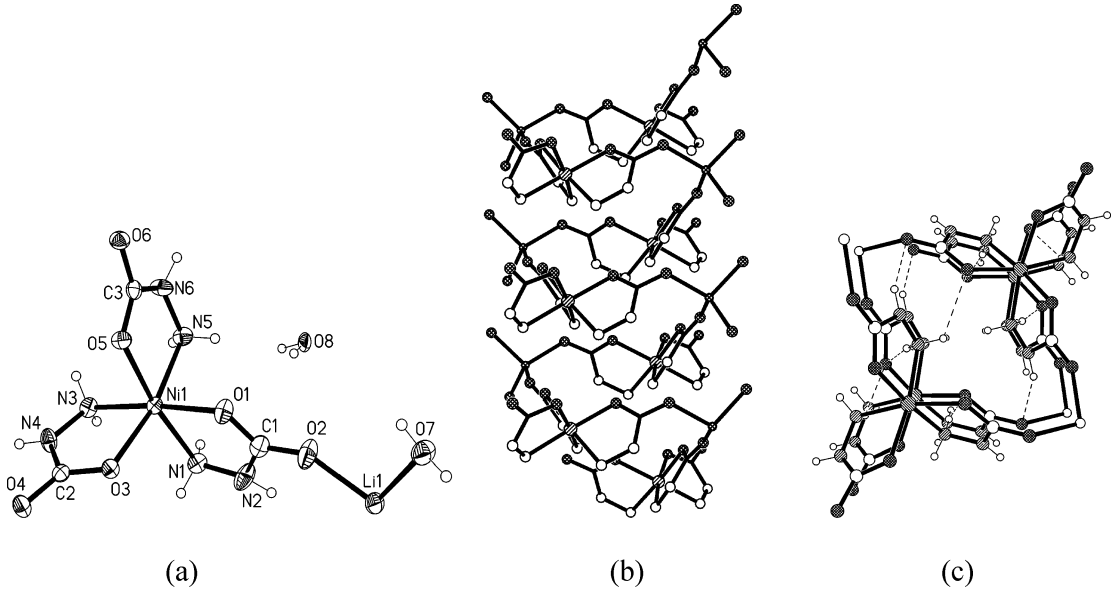

Figure 1. (a) Structure of the contents in the asymmetric unit of **1**. (b) Portion of the helical strand formed by the $LiNi(N_2H_3CO_2)_3$ coordination polymer. (c) Top view of the helical strand viewed from the *b*-axis.

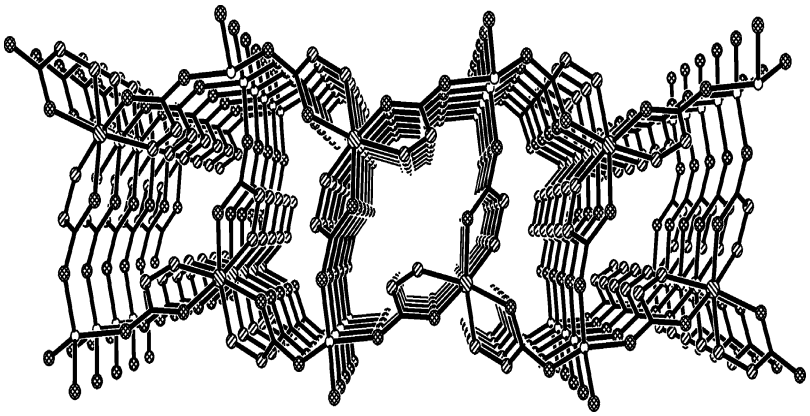

Figure 2. Portion of the 2D bilayer coordination polymeric network structure.

Magnetic Properties. The temperature-dependent magnetic susceptibility of **1** and **2** was studied, as shown in Figure 3. The inverse of the magnetic susceptibility, $1/\chi$, agrees well with paramagnetism.[19] Using the equation $\chi = N\mu_0\mu^2/3kT = M/H$, the magnetic moment μ was estimated to be 2.82 μ_B for Ni and 4.39 μ_B for Co. The value for the Ni^{2+} ion in **1** agrees well with the expected spin-only value of 2.83 μ_B, whereas the value for the Co^{2+} ion in **2** is 15% larger than the spin-only value of 3.87 μ_B. The unquenched orbital moment contribution leads to higher values such as those observed for other Co(II) complexes.[38]

Synthesis and Physical Characterization of $LiNiO_2$ and $LiCoO_2$. Thermogravimetry showed the loss of water in two steps for both precursors. The first one is due to half a molecule of lattice water (weight loss expected, 2.8%; observed, 2.6% for **1** and 2.8% for **2** in the temperature range 25−100 °C). The second weight loss appears to be due to the loss of an aqua ligand (weight loss expected, 5.7%; observed, 8.8% for **1** and 10.0% for **2** in the temperature range 110−240 °C) along with the decomposition of the precursors. The final decomposition occurs in the range of ca. 250−420 °C.

Pure $LiMO_2$ oxides were obtained when the nickel precursors were heated in an oxygen atmosphere at 700 °C for 8 h and cobalt precursors at 700 or 850 °C for 8 h in air. This is attributed to the lower reduction potential of cobalt(III), which makes it easier to oxidize Co^{2+} to Co^{3+} under less critical conditions.[27] The compounds obtained in this way are black powders and consist of a single phase exhibits the characteristic peaks of the layered structures of $LiNiO_2$ and $LiCoO_2$. The XRD patterns are shown in Figure 4. Rietveld refinement of the XRD data of $LiNiO_2$ was carried out assuming the space group $R\bar{3}m$ with an α-$NaFeO_2$ type structure with Li at the *3b* site (0,0, $^1/_2$), transition-metal ions at the *3a* site (0,0,0) and O at the *6c* site (0,0,z) with $z \approx 0.25$. The fitted and difference patterns are shown in Figure 4a. The allowed *hkl* reflections are indicated by vertical bars. The *R*-Bragg and GOF are 3.7 and 1.9, respectively. The refined *z* value is 0.259. The refinement shows that about 4 at % of the Ni ions occupy the Li sites in the Li layer. Accordingly, the relative intensity ratio of (003) and (104) reflections, which is sensitive to the Ni-ion occupancy in the Li layer, is less than unity. The Rietveld refined hexagonal *a* and *c* lattice parameters of $LiNiO_2$ are 2.877(5) and 14.201(4) Å, respectively, which are in good agreement

(38) Kumagai, H.; Kepert, C.; Kurmoo, M. *Inorg. Chem.* **2002**, *41*, 3410.

Table 2. Selected Bond Distances (Å) and Angles (deg) for 1 and 2

	Ni	Co
M(1)−O(1)	2.044(2)	2.060(2)
M(1)−O(3)	2.036(2)	2.063(1)
M(1)−O(5)	2.061(2)	2.096(2)
M(1)−N(1)	2.078(3)	2.139(2)
M(1)−N(3)	2.073(2)	2.146(2)
M(1)−N(5)	2.083(3)	2.138(2)
Li(1)−O(2)	1.919(5)	1.922(4)
Li(1)−O(4)[b]	1.961(6)	1.962(4)
Li(1)−O(6)[a]	1.933(7)	1.940(5)
Li(1)−O(7)	1.994(6)	1.991(5)
N(1)−N(2)	1.413(4)	1.417(3)
O(1)−M(1)−O(3)	95.17(8)	96.65(7)
O(1)−M(1)−O(5)	91.25(8)	91.81(6)
O(3)−M(1)−O(5)	91.04(8)	91.65(6)
O(1)−M(1)−N(5)	92.69(10)	95.57(8)
O(3)−M(1)−N(5)	168.34(9)	164.50(7)
O(5)−M(1)−N(5)	80.18(9)	78.45(7)
O(1)−M(1)−N(1)	79.87(9)	78.17(7)
O(3)−M(1)−N(1)	93.10(9)	95.61(7)
O(5)−M(1)−N(1)	170.49(9)	168.22(7)
N(5)−M(1)−N(1)	96.76(10)	96.20(8)
O(1)−M(1)−N(3)	174.75(10)	173.41(7)
O(3)−M(1)−N(3)	80.40(9)	78.27(6)
O(5)−M(1)−N(3)	91.64(9)	92.52(7)
N(5)−M(1)−N(3)	92.12(11)	90.16(8)
N(1)−M(1)−N(3)	97.49(10)	98.02(8)
O(2)−Li(1)−O(6)[a]	110.1(4)	109.3(3)
O(2)−Li(1)−O(4)[b]	104.3(2)	104.5(2)
O(6)[a]−Li(1)−O(4)[b]	123.9(2)	123.8(2)
O(2)−Li(1)−O(7)	101.0(2)	100.5(2)
O(6)[a]−Li(1)−O(7)	108.8(2)	109.7(2)
O(4)[b]−Li(1)−O(7)	106.4(4)	106.5(3)

[a] Symmetry transformations used to generate equivalent atoms: $x-1$, y, z. [b] Symmetry transformations used to generate equivalent atoms: $-x+1$, $y+{}^1/_2$, $-z+1$.

Table 3. Selected Hydrogen Bond Parameters in 1 and 2

D−H	d(D−H) (Å)	d(H···A) (Å)	∠DHA (deg)	d (D···A)	A	symmetry
Compound **1**						
N1−H1B	0.84(3)	2.26(3)	171(3)	3.088(3)	O1	$[x, y-1, z]$
N2−H2	0.86(2)	2.22(3)	146(2)	2.966(4)	O4	$[-x+1, y-{}^1/_2, -z+1]$
N3−H3A	0.84(3)	2.34(2)	165(2)	3.161(3)	O4	$[-x+2, y-{}^1/_2, -z+1]$
N3−H3B	0.84(3)	2.15(2)	166(2)	2.974(3)	O3	$[x, y-1, z]$
N4−H4	0.85(4)	2.26(4)	160(3)	3.070(3)	O5	$[-x+2, y-{}^1/_2, -z+1]$
N5−H5A	0.83(3)	2.10(3)	160(3)	2.898(5)	O8	$[-x+1, y+{}^1/_2, -z+2]$
N6−H6	0.86(2)	2.14(2)	163(2)	2.964(3)	O6	$[-x+2, y-{}^1/_2, -z+2]$
O7−H7A	0.90(1)	1.93(1)	155(1)	2.768(5)	O8	$[-x+1, y+{}^3/_2, -z+2]$
O7−H7B	0.90(1)	1.88(1)	172(2)	2.770(5)	O6	$[x-1, y+1, z]$
O8−H8A	0.90(5)	1.85(4)	155(4)	2.69(1)	O8	$[-x+1, y+{}^1/_2, -z+2]$
O8−H8B	0.90(5)	1.83(4)	159(4)	2.69(1)	O8	$[-x+1, y-{}^1/_2, -z+2]$
Compound **2**						
N1−H1B	0.88(2)	2.23(2)	159(2)	3.063(3)	O1	$[x, y+1, z]$
N2−H2	0.90(2)	2.20(3)	143(2)	2.970(3)	O4	$[-x+1, y+{}^1/_2, -z+1]$
N3−H3A	0.88(2)	2.33(2)	162(2)	3.177(2)	O4	$[-x, y+{}^1/_2, -z+1]$
N3−H3B	0.89(2)	2.11(2)	163(2)	2.972(2)	O3	$[x, y+1, z]$
N4−H4	0.88(3)	2.25(3)	158(3)	3.086(3)	O5	$[-x, y+{}^1/_2, -z+1]$
N5−H5A	0.87(3)	2.08(3)	161(3)	2.917(4)	O8	$[-x+1, y-{}^1/_2, -z]$
N6−H6	0.89(2)	2.11(2)	160(2)	2.958(2)	O6	$[-x, y+{}^1/_2, -z]$
O7−H7A	0.90(1)	1.95(1)	156(1)	2.798(4)	O8	$[-x+1, y-{}^3/_2, -z]$
O7−H7B	0.90(1)	1.89(1)	171(1)	2.777(3)	O6	$[x+1, y-1, z]$
O8−H8A	0.90(4)	1.89(4)	158(3)	2.740(8)	O8	$[-x+1, y-{}^1/_2, -z]$
O8−H8B	0.90(4)	1.87(4)	162(3)	2.740(8)	O8	$[-x+1, y+{}^1/_2, -z]$

with those reported by Arai et al.[10] and in the JCPDS No. 74-0919.

The XRD patterns of $LiCoO_2$ prepared at 700 and 850 °C in air are shown in Figure 4b, along with the (*hkl*) Miller indices. The lattice parameters were obtained by the least-squares fitting of select (*hkl*) and 2θ values. At 700 °C, a = 2.817(4) Å, c = 14.159 (2) Å; at 850 °C, a = 2.819(3) Å, c = 14.062(2) Å. These values are in good agreement with

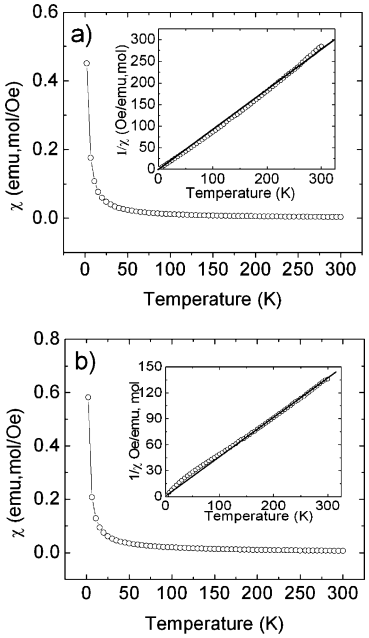

Figure 3. Variable temperature plot for magnetic susceptibility, χ, and its reciprocal magnetic susceptibility, $1/\chi$ (inset), for (a) $[Li(H_2O)Ni(N_2H_3CO_2)_3]\cdot 0.5H_2O$ (**1**) and (b) $[Li(H_2O)Co(N_2H_3CO_2)_3]\cdot 0.5H_2O$ (**2**).

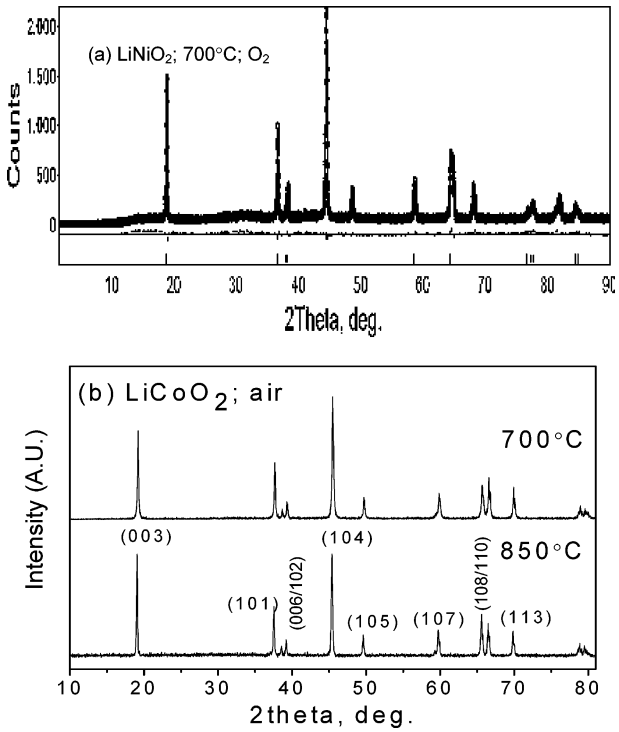

Figure 4. Powder X-ray diffraction patterns (Cu Kα radiation). (a) $LiNiO_2$. Circles are experimental data, and continuous lines represent the Rietveld refinement fitted pattern. The difference pattern and positions of allowed reflections (vertical lines) are also shown. (b) $LiCoO_2$. Synthesis temperature and Miller indices are shown.

those reported in the literature[12] and in the JCPDS No. 44-0145. Clear splitting of the XRD lines assigned to the peak pairs with the Miller indices (006, 102) and (108,110) in $LiCoO_2$ is an indication of a well-ordered layer structure (Figure 4b). Therefore, we conclude that combustion of **1** and **2** to yield $LiMO_2$ with the desired layer structure requires high temperatures (≥700 °C) and also an oxygen atmosphere in the case of **1**. Such conditions are required because the

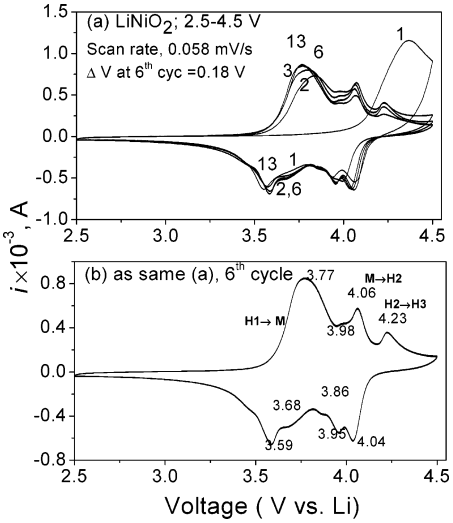

Figure 5. Cyclic voltammograms of $LiNiO_2$ prepared at 700 °C in an O_2 atmosphere with a scan rate of 0.058 mV s^{-1}; numbers refer to cycle numbers. Li metal was the counter and reference electrode. (a) Voltage range 2.5−4.5 V. (b) Same as panel a, with the 6th cycle in a slightly expanded scale; numbers refer to voltages. Structural transitions (H1, M, H2, H3) are also shown.

reaction underwent a phase change upon combustion; hence, significant energy input is required for lattice reconstruction to take place. It must be mentioned that this finding is contrary to our initial assumption that the decomposition of the precursor at low temperatures would yield the desired layered $LiMO_2$. SEM photographs of $LiNiO_2$ and $LiCoO_2$ (850 °C synthesis) showed agglomerates of submicrometer-sized particles of $LiNiO_2$ and platelets with a layer structure in the case of $LiCoO_2$.

Electrochemical Studies. *Cyclic Voltammetry.* The cyclic voltammograms (CV) of the cells were recorded on cells with $LiMO_2$ as cathodes vs Li metal, which acted as the counter and reference electrode, in the ranges 2.5−4.4 and 2.5−4.5 V at ambient temperature (25 °C) at a scan rate of 58 or 52 μV/s up to 13 cycles. These scan rates are sufficiently small so that they can be considered close to the slow scan cyclic voltammograms (SSCV) and can reveal fine features related to the intercalation/deintercalation stages and phase transitions occurring in the cathodes.[39,40] The first cycle CV of $LiNiO_2$ shows a broad anodic peak (deintercalation of Li ions) at ∼4.36 V, whereas the main cathodic peak (intercalation of Li ions) peak is at ∼3.54 V (Figure 5a). In the second cycle, the anodic peak shifts to a lower voltage (∼3.83 V). The shift in the anodic peak voltage is an indication of the formation of the electrode in the first cycle, wherein the active material makes good electrical contact with the current collector and the liquid electrolyte. The shifts in the main anodic and cathodic peak voltages are stabilized by the sixth cycle, at 3.77 and 3.59 V (±0.02), respectively (Figure 5b). The hysteresis (ΔV = the difference between the sixth anodic and cathodic peak voltages) is 0.18 V, indicating good reversibility of the charge−discharge reaction.

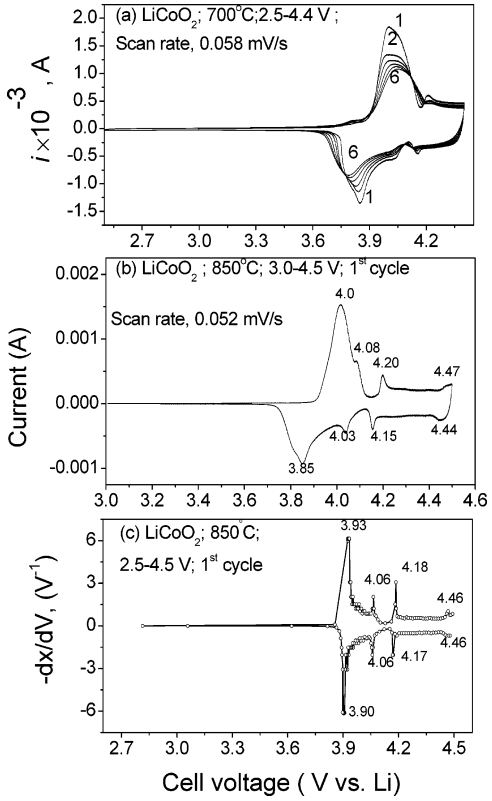

Figure 6. (a,b) Cyclic voltammograms of $LiCoO_2$. Synthesis temperature, voltage ranges, and scan rate are indicated. The numbers in (a) refer to cycle number and those in (b) refer to the voltages. (c) Differential capacity (dx/dV) vs potential (V) plot of $LiCoO_2$ extracted from Figure 8b (1st cycle).

The major anodic/cathodic peaks at 3.77/3.59 V are assigned to the $Ni^{3+/4+}$ redox couple and to the reversible hexagonal (H1) ↔ monoclinic (M) structural transition in $LiNiO_2$. In addition, there are well-defined anodic and cathodic peaks in the voltage range 3.9−4.2 V (Figure 5b). These can be assigned to the reversible M ↔ H2 and H2 ↔ H3 crystallographic transitions, where H2 and H3 refer to the phases with hexagonal structure but slightly different lattice parameters. The presently observed anodic/cathodic peak voltages agree very well with the corresponding values reported by several groups on $LiNiO_2$ on the basis of the SSCV,[39,40] CV,[41] and differential capacity (dx/dV) vs voltage (V) plots.[42−45] It is now well-known that the above reversible phase transitions are responsible for the capacity degradation when $LiNiO_2$ is cycled with an upper cutoff voltage of 4.3 or 4.5 V.

The CVs of $LiCoO_2$ prepared at 700 °C in the voltage range 2.5−4.4 V up to 6 cycles are shown in Figure 6a. During the first cycle, the major anodic peak occurs at just below 4.0 V vs Li, followed by a small low-intensity peak at 4.2 V. The cathodic scan reveals peaks at 4.15 and 4.05 V and a high-intensity peak at 3.85 V. During subsequent

(39) Aurbach, D.; Levi, M. D.; Levi, E.; Teller, H.; Markovsky, B.; Salitra, G.; Heider, U.; Heider, L. *J. Electrochem. Soc.* **1998**, *145*, 3024.
(40) Levi, E.; Levi, M. D.; Salitra, G.; Aurbach, D.; Oesten, R.; Heider, U.; Heider, L. *Solid State Ionics* **1999**, *126*, 97.
(41) Cho, J.; Jung, H. S.; Park, Y. C.; Kim, G. B.; Lim, H. S. *J. Electrochem. Soc*. **2000**, *147*, 15.
(42) Li, W.; Reimers, J. N.; Dahn, J. R. *Solid State Ionics* **1993**, *67*, 123.
(43) Barker, J.; Koksbang, R.; Saidi, M. Y. *Solid State Ionics* **1996**, *89*, 25.
(44) Arai, H.; Okada, S.; Sakurai, Y.; Yamaki, J.-I. *Solid State Ionics* **1997**, *95*, 275.
(45) Delmas, C.; Ménétrier, M.; Croguennec, L.; Levasseur, S.; Peres, J. P.; Pouillerie, C.; Prado, G.; Fournes, L.; Weill, F. *Int. J. Inorg. Mater.* **1999**, *1*, 11.

cycles, no major shifts occur in the voltages of the peaks. The first cycle CV of $LiCoO_2$ prepared at 850 °C in the voltage range 2.5−4.5 V at the scan rate of 0.052 mV/s is shown in Figure 6b. Interestingly, the formation cycle is not shown in the CV, and the peak positions are well-resolved in Figure 6b in comparison to those in Figure 6a. The major anodic/cathodic peaks at 4.0/3.85 V correspond to the reversible Li ion intercalation/deintercalation reactions, involving the $Co^{3+/4+}$ couple, in addition to the coexistence of two $Li_{1-x}CoO_2$ phases with $x \geq 0.94$ (semiconducting) and $x \leq 0.75$ (metallic).[12,44,45−47]

Sharp and low-intensity peaks at 4.08, 4.20, and 4.47 (±0.02) V are also seen in the anodic scan in Figure 6b. The corresponding cathodic peaks are at 4.03, 4.15, and 4.44 (±0.02) V. These have been observed in the SSCV,[39] CV,[48,49] and $(dx/dV)-V$ plots [46,50] by others in the literature and assigned to the reversible H1 ↔ M, M ↔ H1, and H1 ↔ (H1−3) crystallographic transitions, respectively.[46,50] Here H1 and (H1−3) refer to the phases with hexagonal structure but slightly different lattice parameters. The peak positions remained unchanged on repeated cycling, except that the peak areas under the major anodic/cathodic peaks decreased (not shown in figure), similar to in Figure 6a. Thus, an unoptimized $LiCoO_2$ in which the structural transitions are not suppressed shows capacity-fading on cycling to ≥4.2 V vs Li. This is the reason commercial LIB with a $LiCoO_2$ cathode and graphite anode is cycled only to an upper cutoff voltage of ≤4.2 V.

Galvanostatic Charge−Discharge Cycling. Charge−discharge cycling of the cells with $LiMO_2$ cathodes was carried out up to 20 cycles at a current density of 20 mA g^{1-} at ambient temperature. The voltage ranges were 2.5−4.3 and 2.5−4.5 V. The voltage-capacity profiles of $LiNiO_2$ are shown in Figure 7a,b. For clarity, only profiles of select cycles are shown. During the first-charge process, the voltage suddenly increased to ∼3.8−3.9 V from the open circuit voltage (∼3.0 V), followed by a voltage plateau to about ∼20 mA h g^{-1} was reached and the voltage then gradually increased to the upper cutoff voltage. Similarly, during the first-discharge, the voltage dropped to 4.1−4.2 V with both the 4.3 and 4.5 V cutoffs. The voltage profiles stabilized after 6−10 cycles. The voltage plateaus in the charge and discharge profiles at 4.05 and 4.2 V, more clearly seen in Figure 7b, indicate a two-phase coexistence and are due to the M ↔ H2 and H2 ↔ H3 crystallographic transitions. These were observed as peaks in the CV curves at the respective voltages (Figure 5b). With the 4.3 V cutoff, the first charge and discharge capacities are 168 and 128 mA h g^{-1}, respectively, whereas with the 4.5 V cutoff, the corresponding values are 206 and 163 mA h g^{-1}. The irreversible capacity losses (ICL) during the first cycle are 40 and 43 mA h $^{-1}$, respectively, with 4.3 and 4.5 V cutoffs. Similar

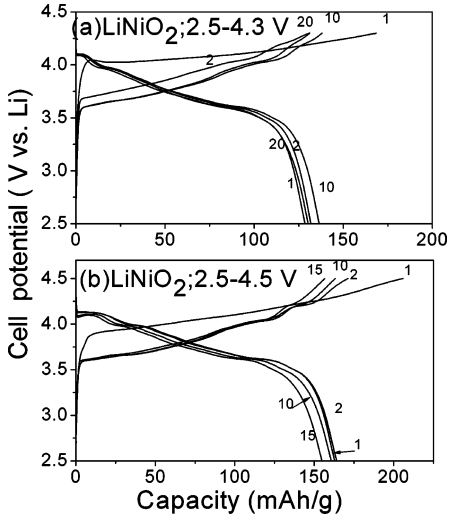

Figure 7. Voltage vs capacity profiles of $LiNiO_2$: (a) voltage range 2.5−4.3 V, (b) voltage range 2.5−4.5 V. Current rate was 20 mA g^{1-}. The numbers refer to cycle numbers.

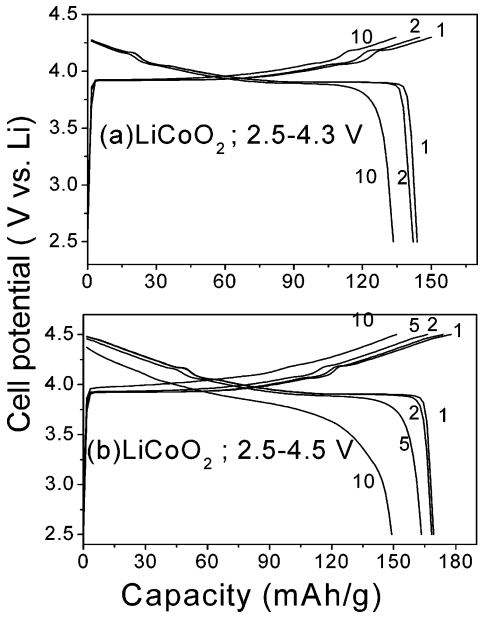

Figure 8. Voltage vs capacity plots of $LiCoO_2$ prepared at 850 °C: (a) voltage range 2.5−4.3 V, (b) voltage range 2.5−4.5 V. Current rate was 20 mA g^{1-}. The numbers refer to cycle numbers.

capacity values and high ICL have also been reported by other groups in the literature.[1,2,9,10,41] The ICL is attributed to electrode formation and to the irreversible oxidation of some of the Ni^{2+} ions that occupy the Li layer during the synthesis of $LiNiO_2$. As is evident from panels a and b of Figure 7, the charge and discharge capacities decrease gradually during the 10−15 (or 20) cycles, similar to other reports in the literature, and are ascribed to the reversible structural transitions taking place in $LiNiO_2$, which must be suppressed for better cathodic performance.[1,2,10,41]

The voltage-capacity profiles of $LiCoO_2$ prepared at 850 °C in the ranges 2.5−4.3 and 2.5−4.5 V are shown in panels a and d, respectively, of Figure 8. The current density was 20 mA g^{-1}, which corresponds to 0.13 C (1 C = 160 mA g^{-1}). The first-charge profile clearly shows voltage plateaus at ∼3.9, 4.05, and 4.18 V, corresponding to the coexistence of two phases with differing x values in $Li_{1-x}CoO_2$. To clearly

(46) Chen, Z.; Lu, Z.; Dahn, J. R. *J. Electrochem. Soc*. **2002**, *149*, 1604.
(47) Levasseur, S.; Ménétrier, M.; Shao-Horn, Y.; Gautier, L.; Audemer, A.; Demazeau, G.; Largeteau, A.; Delmas, C. *Chem. Mater*. **2003**, *15*, 348.
(48) Broussely, M.; Perton, F.; Labat, J.; Staniewicz, R. J.; Romero, A. *J. Power Sources* **1993**, *43*−*44*, 209.
(49) Yoon, W.-S.; Kim, K.-W. *J. Power Sources* **1999**, *81*−*82*, 517.
(50) Chen, Z.; Dahn, J. R. *Electrochim. Acta* **2004**, *49*, 1079.

delineate the voltage plateaus, we extracted differential capacity (dx/dV) vs V plots from the data; they are shown in Figure 6c. In these plots, the sharp peaks correspond to two-phase regions, whereas minima or smoothly varying profiles represent single-phase Li intercalation/deintercalation in the electrode.[42−44,46,50] As can be seen, there is almost a one-to-one correspondence between the peaks and the voltage values in the CV and (dx/dV) vs V plots (Figure 6). Even though the first charge and discharge capacities are smaller compared to $LiNiO_2$, better reversibility and coulombic efficiency is shown by $LiCoO_2$ (Figure 8a,b). Thus, with a 4.3 V cutoff, the first charge and discharge capacities are 150 and 144 mA h g^{-1}, respectively, with an ICL of only 6 mA h g^{-1}. With a 4.5 V cutoff, the corresponding values are 178 and 169 mA h g^{-1} (ICL = 9 mA h g^{-1}). However, capacity fading is evident regardless of the voltage cutoff values from 2 to 10 cycles. This can be explained as being due to the reversible structural transitions (H1 ↔ M and M ↔ H1) exhibited by $LiCoO_2$.[12,50] The slight unit-cell volume changes associated with these phase transitions shown by $LiMO_2$, M = Ni and Co, produce an electrochemical grinding effect and deterioration of the electrode material's electrical contact with other particles and the current collector, leading to degradation of capacity on long-term cycling. Thus, the electrochemical behavior of the presently synthesized $LiMO_2$ is in tune with reports by several groups in the literature and emphasizes the need for optimization of the preparation conditions and precursors.

Conclusions

Heterobimetallic complexes of hydrazidocarbonate ligand, $[Li(H_2O)M(N_2H_3CO_2)_3]\cdot 0.5H_2O$ (M = Ni (**1**) and Co (**2**)) have been synthesized and characterized by X-ray crystallography. The solid-state structures of these complexes contain fused helical strands that form interesting 2D coordination polymeric structures with extensive hydrogen bonding. Both **1** and **2** exhibit paramagnetic behavior in the variable temperature magnetic studies. Because both lithium and transition metal (nickel or cobalt) are incorporated in to the precursors in a 1:1 mole ratio and because hydrazido carbonate ligands have been successfully employed in synthesizing the oxide materials, they have been tested as single-source precursors for $LiNiO_2$ and $LiCoO_2$ battery materials. Pyrolysis of the precursor compound **1** at 700 °C in an O_2 atmosphere yielded single-phase $LiNiO_2$, whereas precursor **2** yielded $LiCoO_2$ on heating at 700 or 850 °C in air. The XRD and SEM of both oxides show a characteristic hexagonal layered structure and morphology. Cathodic behavior of $LiNiO_2$ and $LiCoO_2$ has been tested by cyclic voltammetry and galvanostatic charge−discharge cycling up to 20 cycles in the voltage ranges 2.5−4.3 and 2.5−4.5 V. Results are in tune with the reported data in the literature. These preliminary studies show that the single-source precursor route is a promising one for the synthesis of ternary metal oxides $LiMO_2$ and it might be suitable for making these battery materials on an industrial scale.

Acknowledgment. We thank NUS for its generous financial support. This work is taken partially from the B.S. honors thesis of Ms. S. L. Tey.

Supporting Information Available: CIF data for **1** and **2**. This material is available free of charge via the Internet at http://pubs.acs.org.

CM0523891